

An optoelectronic microwave synthesizer with frequency tunability and low phase noise

Received: 29 March 2024

Accepted: 23 October 2024

Published online: 11 December 2024

 Check for updates

Igor Kudelin^{1,2,3}✉, Pedram Shirmohammadi⁴, William Groman^{1,2,3}, Samin Hanifi⁴, Megan L. Kelleher^{2,3}, Dahyeon Lee^{2,3}, Takuma Nakamura^{2,3}, Charles A. McLemore^{2,3}, Alexander Lind^{1,3}, Dylan Meyer¹, Junwu Bai⁴, Joe C. Campbell⁴, Steven M. Bowers⁴, Franklyn Quinlan^{1,3} & Scott A. Diddams^{1,2,3}✉

Communication, navigation and radar systems rely on frequency-tunable and low-noise microwave sources. Compared to electronic microwave synthesizers, photonic systems that leverage high spectral purity lasers and optical frequency combs can generate microwaves with exceptionally low phase noise. However, photonic approaches lack frequency tunability and have substantial size, weight and power requirements, which limit wider application. Here we address these shortcomings with a hybrid optoelectronic approach that combines simplified optical frequency division with direct digital synthesis to produce tunable low-phase-noise microwaves across the entire X-band (8–12 GHz). This resulted in phase noise at 10 GHz of -156 dBc Hz⁻¹ at 10 kHz offset and fractional frequency instability of 1×10^{-13} at 0.1 s. Spot-tuning away from 10 GHz by ± 500 MHz, ± 1 GHz or ± 2 GHz yielded phase noise at 10 kHz offset of -150 , -146 and -140 dBc Hz⁻¹, respectively. Our synthesizer architecture is compatible with integrated photonic implementations and, thus, could be integrated in a chip-scale package.

Microwave signals with low phase and timing noise are critical for several fields including timekeeping, navigation, communications and radar-based sensing. The demand for improved performance in these applications requires microwave frequency synthesis that has both low timing jitter and broad tunability. For example, microwave spectroscopy (which is critical for atomic clocks¹ and radio astronomy²) requires precise and low-noise signals but minimal frequency tuning, whereas communication systems often require fast frequency hopping and, thus, low phase noise of the carrier signal because it affects the error vector magnitude and bit error rate^{3–5}. Radar relies on both frequency agility and low noise^{6–9}, with low

phase noise improving the detection probability as well as imaging accuracy and quality¹⁰.

Microwave synthesis is also used in fields such as metrology, sensors and navigation systems, which highlights the importance of developing robust and low-noise microwave synthesis that covers a broad frequency range. However, there is a fundamental trade-off between low noise and broad and fast tunability. Conventional electronic synthesizers introduce frequency tunability with multiple electronic up-converters and local oscillators, but these tuning elements introduce noise that is multiplicative as the frequency increases. In contrast, the best photonic-based synthesis uses frequency division

¹Electrical Computer & Energy Engineering, University of Colorado Boulder, Boulder, CO, USA. ²Department of Physics, University of Colorado Boulder, Boulder, CO, USA. ³National Institute of Standards and Technology, Boulder, CO, USA. ⁴Department of Electrical and Computer Engineering, University of Virginia, Charlottesville, VA, USA. ✉e-mail: igor.kudelin@colorado.edu; scott.diddams@colorado.edu

to create microwaves with exceptional phase-noise performance but with restricted tunability that is often in the range of 0.1%^{11–15}.

In this article, we report a microwave synthesizer that combines the low noise of photonic-based frequency division with broadband electronic digital tuning. Our synthesizer consists of a low-noise photonic oscillator at 10 GHz generated using two-point optical frequency division (2P-OFD)^{16–18}. This provides a fixed 10 GHz microwave signal with phase noise of -156 dBc Hz⁻¹ at 10 kHz offset and fractional frequency instability of 1×10^{-13} . The low-noise signal is then used as the reference clock for a direct digital synthesizer (DDS). The output of the DDS is mixed with the clock itself to provide tunable low-noise microwaves across the entire X-band (8–12 GHz).

In contrast to previous works^{19,20}, we incorporate simplifications to the photonic system that make it compatible with recent advances in chip-level integration^{17,18,21–25}. Using 2P-OFD results in a lower division factor, but it enables a large reduction in the size and power requirements compared to traditional optical frequency division (OFD) approaches^{11,12,19}. Our synthesizer generates microwaves with phase noise at 10 kHz offset of -150 dBc Hz⁻¹ in the tuning range ± 500 MHz (from the 10 GHz carrier signal), -146 dBc Hz⁻¹ at ± 1 GHz and -140 dBc Hz⁻¹ at ± 2 GHz. At the same time, the DDS allows tuning with microhertz resolution and speeds of tens of nanoseconds. We also increase the continuous tuning range by up to a factor of 4 and improve the phase noise by 10 dB compared with previous systems^{19,20}. Our system is also amenable to chip-scale integration^{18,26–32} to address the demanding requirements of modern applications beyond the laboratory environment.

Low-noise microwave generation

In our realization of 2P-OFD, the low phase noise of continuous wave (CW) lasers is transferred to an optical frequency comb and its microwave-rate mode spacing. This is achieved by first narrowing the linewidth of the CW lasers through active stabilization of their frequencies to a high quality (Q) factor with a Fabry–Pérot (FP) cavity³³. The FP cavity plays a crucial role in low-noise microwave generation with 2P-OFD by providing the phase and frequency reference of the generated microwave signal. The lowest noise can be achieved with a long FP cavity length^{34,35} or with cryogenic cooling³⁶. However, rejection of the thermal noise that is common to separate modes of the cavity, hereafter called common mode rejection, allowed us to take advantage of miniature FP cavities to reduce the system size^{37,38}. We employ an FP cavity that is only 6.3 mm long with ultralow-loss mirrors, yielding a cavity free-spectral range of 23.6 GHz and $Q \approx 5$ billion. The fractional frequency instability is as low as 3×10^{-14} with 1 s of averaging³⁸. The phase noise of the lasers that are stabilized to the cavity inherit the thermal-limited cavity length stability for offset frequencies below 10 kHz.

As shown in the experimental set-up in Fig. 1, two lasers with frequencies ν_{1555} and ν_{1545} and a frequency separation of 1.3 THz are stabilized to different modes of the FP cavity. This gap, which is $55\times$ the cavity free-spectral range, is then divided down with an electro-optic (EO) frequency comb. The EO comb is generated by phase modulating a 1,550 nm CW laser (ν_{1550}) with the amplified output of a voltage-controlled oscillator (VCO) at modulation frequency $f_m = 10$ GHz (ref. 39) (Extended Data Fig. 1). The comb frequency spacing (repetition rate) is given by $f_{\text{rep}} = f_m$. The optical spectra of the comb and the two CW lasers are shown in Fig. 2a.

2P-OFD is implemented by heterodyning the cavity-stabilized optical references ν_{1555} and ν_{1545} with the closest comb lines $\nu_{1550} - n f_{\text{rep}}$ and $\nu_{1550} + m f_{\text{rep}}$, where n and m are positive integers. This yields two beat notes $f_{b1} = \nu_{1555} - \nu_{1550} + n f_{\text{rep}}$ and $f_{b2} = \nu_{1545} - \nu_{1550} - m f_{\text{rep}}$, which are further mixed to provide an intermediate frequency $f_{\text{IF}} = f_{b2} - f_{b1} = \nu_{1545} - \nu_{1555} - (n + m) f_{\text{rep}}$. The correct choice of the sum of or difference between f_{b1} and f_{b2} depends on the frequency positions of the CW lasers relative to the comb lines. Conveniently, f_{IF} does not depend on the centre frequency of the EO comb, thus allowing the use of a free-running laser for ν_{1550} .

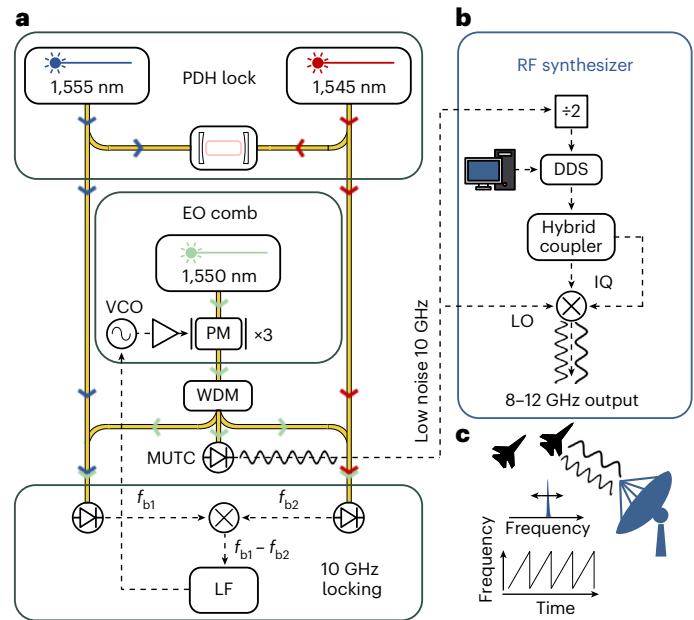


Fig. 1 | Experimental set-up. **a**, Two CW fibre lasers operating at 1,545 nm and 1,555 nm are locked to a millimetre-scale FP cavity with the Pound–Drever–Hall technique. The comb is generated by modulating the light from a 1,550 nm CW laser at 10 GHz. The EO comb is split in a wavelength-division multiplexer to provide the beat notes (f_{b1} and f_{b2}) with the reference lasers. Part of the EO comb is detected in a modified uni-travelling carrier detector to provide a low-noise microwave at f_{rep} . The beat frequencies between the CW lasers and the EO comb are mixed together to provide the error signal, which is conditioned with a loop filter and used to stabilize the VCO and the EO comb mode spacing. **b**, The stabilized 10 GHz is frequency-divided by two and serves as the clock signal for a DDS. The DDS output is split in the hybrid coupler to provide two signals with 90° relative phase shift. These signals are mixed with the original 10 GHz in an IQ mixer for single-sideband generation. By tuning the DDS frequency, the synthesizer output covers the entire X-band (8–12 GHz). **c**, Illustration of applications that rely on low-noise frequency sweeping, such as radar and navigation systems. LF, loop filter; MUTC, modified uni-travelling carrier; PDH, Pound–Drever–Hall; WDM, wavelength-division multiplexer; PM, phase modulator; LO, local oscillator.

To complete the comb stabilization, the intermediate frequency is compared to a reference oscillator f_{ref} to generate an error signal that is conditioned and fed to the 10 GHz VCO.

Once the servo loop is closed, the frequency f_{rep} is given by:

$$f_{\text{rep}} = \frac{(\nu_{1545} - \nu_{1555}) + f_{\text{IF}}}{(n + m)}. \quad (1)$$

The denominator $(n + m)$ is the number of comb modes between the CW lasers and is responsible for the frequency division and corresponding noise reduction due to OFD. In terms of the power spectral density of the phase noise, this reduction is equal to $20 \log [(\nu_{1545} - \nu_{1555}) / f_{\text{rep}}] = 20 \log [1.3 \text{ THz} / 10 \text{ GHz}] = 42$ dB. This division reduces the noise contributions of the relative stability of the reference lasers, $(\nu_{1545} - \nu_{1555})$, and f_{IF} .

As both lasers are locked to the same cavity, a substantial part of their noise is highly correlated. This improves the relative phase noise by up to 40 dB due to the common mode rejection of the cavity noise^{40–42}. The relative phase noise is, thus, reduced to below the thermal noise of the cavity to the limit imposed by the residual noise of the individual laser locking circuits. Thus, with the exception of improved long-term stability, there is little advantage to using a larger FP cavity with lower thermal noise. Besides, smaller FP cavities are typically less sensitive to acoustic noise^{43,44}.

The output of the servo-controlled VCO provides direct access to the 10 GHz signal. In principle, this signal could be at the power level of several watts if taken at the termination port of one of the modulators (Methods and Extended Data Fig. 1). As we used three pairs of radio-frequency (RF) amplifiers and EO modulators in parallel, the control feedback loop for comb stabilization accounts for all additive noise of the RF amplifiers. However, the 10 GHz signal taken after just one of the amplifiers would not have the servo-suppressed noise of the other RF amplifiers. That would limit the achievable noise to be greater than that of the reference lasers ($\nu_{1545} - \nu_{1555}$) (Methods and Extended Data Fig. 2). Instead, to suppress the noise of all the RF amplifiers and obtain the lowest-noise 10 GHz signal, we photodetect the output of the EO comb with a high-power and high-linearity modified uni-travelling carrier photodiode^{32,45}. Fibre dispersion and optical filtering of the spectrum in the wavelength-division multiplexor transform the phase modulation that creates the EO comb into an amplitude-modulated signal that can be photodetected with sufficient signal-to-noise ratio.

As shown in Fig. 2b, in this configuration we achieve phase noise of -156 dBc Hz⁻¹ at 10 kHz offset frequency. At higher offset frequencies, the microwave performance is limited by the phase locking of f_{IF} (grey curve in Fig. 2b). Reducing the noise in this frequency range would require broader bandwidth servo control of f_{IF} . At offset frequencies below 100 kHz, the phase noise is limited by the relative stability of the CW lasers, as shown by the red curve in Fig. 2b (Methods and Extended Data Fig. 3). Further improvement of the relative phase noise of the reference CW lasers, and the resulting 10 GHz, could be achieved by using optimized servo controls to further reduce the residual noise of the Pound–Drever–Hall locking.

We also characterize the time-domain stability of the 10 GHz microwave signal (Fig. 2c). We measure the minimum in the fractional frequency instability of 1×10^{-13} for an integration time of 0.1 s. At longer averaging times, the instability increases due to the drift of the FP cavity. This drift is mirrored by the drift of a single CW laser as well as the relative instability of the two CW lasers. However, note that the frequency instability between the two CW lasers is higher than the stability of each of the reference CW lasers. We attribute that to the measurement set-up (Methods and Extended Data Fig. 1), which is susceptible to environmental vibrations. All the curves in Fig. 2c are above the previously measured instability limit of the cavity, which is at the level of $2-3 \times 10^{-14}$ (ref. 38).

As indicated in equation (1) and surrounding text, f_{rep} can be tuned with f_{IF} , which assumes a maximum value of f_{rep} through coarse stepwise tuning of the VCO. Nonetheless, when divided by $(n + m) \approx 130$, the tunability is reduced to a small fraction of f_{rep} . This limitation is a common drawback in all OFD systems, but in what follows we show how the tuning range can be substantially increased.

Broad bandwidth tunability with low phase noise

Broad bandwidth tunability of the low-noise 10 GHz microwave is achieved by mixing this signal with the output of a DDS. With reference to Fig. 1b, the low-noise microwave at 10 GHz is frequency-divided by 2 and serves as a reference (clock) for the DDS. The DDS output is then added to (or subtracted from) the original 10 GHz reference using an IQ mixer. As the DDS initially creates the output waveform only at discrete time intervals, its generated output frequency cannot exceed the Nyquist–Shannon sampling theorem limit. For the DDS employed here, the maximum output frequency is 2 GHz, which was $\sim 40\%$ of the reference input $f_{rep}/2$.

The basic architecture of the DDS is shown in Fig. 3a. At each clock cycle, the phase accumulator calculates a new phase value by taking into account both the clock signal frequency f_{clock} and a user-provided tuning word. It then performs a lookup operation to translate this phase information into a digital amplitude that is transformed into an analogue voltage by a digital-to-analogue converter (DAC)⁴⁶. The two main contributions to the phase noise of the DDS output at f_{out} are: (1) the

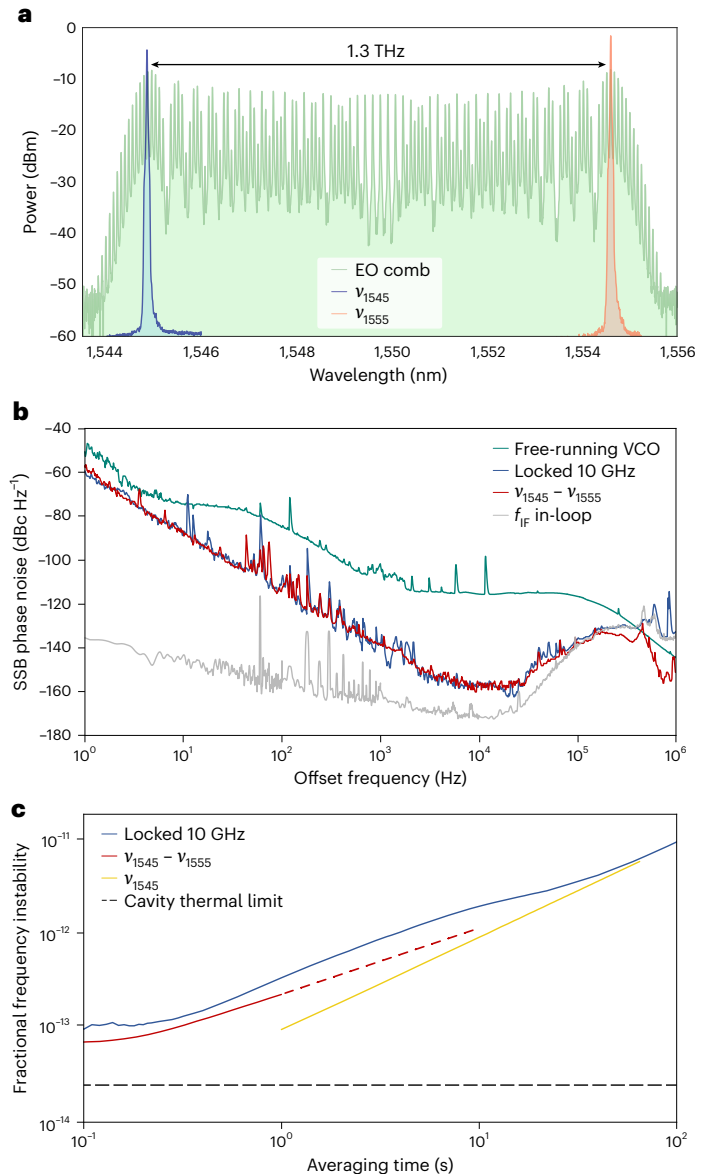


Fig. 2 | EO comb performance. **a**, Optical spectra of the EO comb and reference CW lasers. **b**, Phase noise of the free-running VCO (green), photodetected stabilized 10 GHz (blue), in-loop phase noise of the intermediate frequency locking (light grey) and the relative phase noise of the reference CW lasers ($\nu_{1545} - \nu_{1555}$) spaced by 1.3 THz. This noise is measured independently and decreased by the OFD value of 42 dB (red). **c**, Fractional frequency instability of the stabilized 10 GHz (blue), relative stability of reference CW lasers ($\nu_{1545} - \nu_{1555}$) spaced by 1.3 THz (red), the optical stability of the reference laser (yellow) and the calculated thermal noise limit of the cavity (dashed black).

input clock noise, which is reduced by the ratio $(f_{clock}/f_{out})^2$ and (2) the intrinsic noise originating within the DDS itself, which arises from flicker noise, quantization noise, truncation noise and nonlinearity in the DAC⁴⁷.

Figure 3b shows sample phase noise when the DDS is clocked by the low-noise 5 GHz and its output is set at frequencies between 100 MHz and 2 GHz. For the 100 MHz output, the output noise is limited by the DDS intrinsic noise, reaching -152 dBc Hz⁻¹ at 10 kHz offset frequency. As the DDS frequency increases, the noise of the clock signal started to dominate at offset frequencies above 100 kHz.

The DDS output is summed or differenced with the original 10 GHz microwave in an IQ mixer. The low-noise 10 GHz at f_{rep} is amplified to saturate the mixer, whereas the DDS output is split in a hybrid coupler

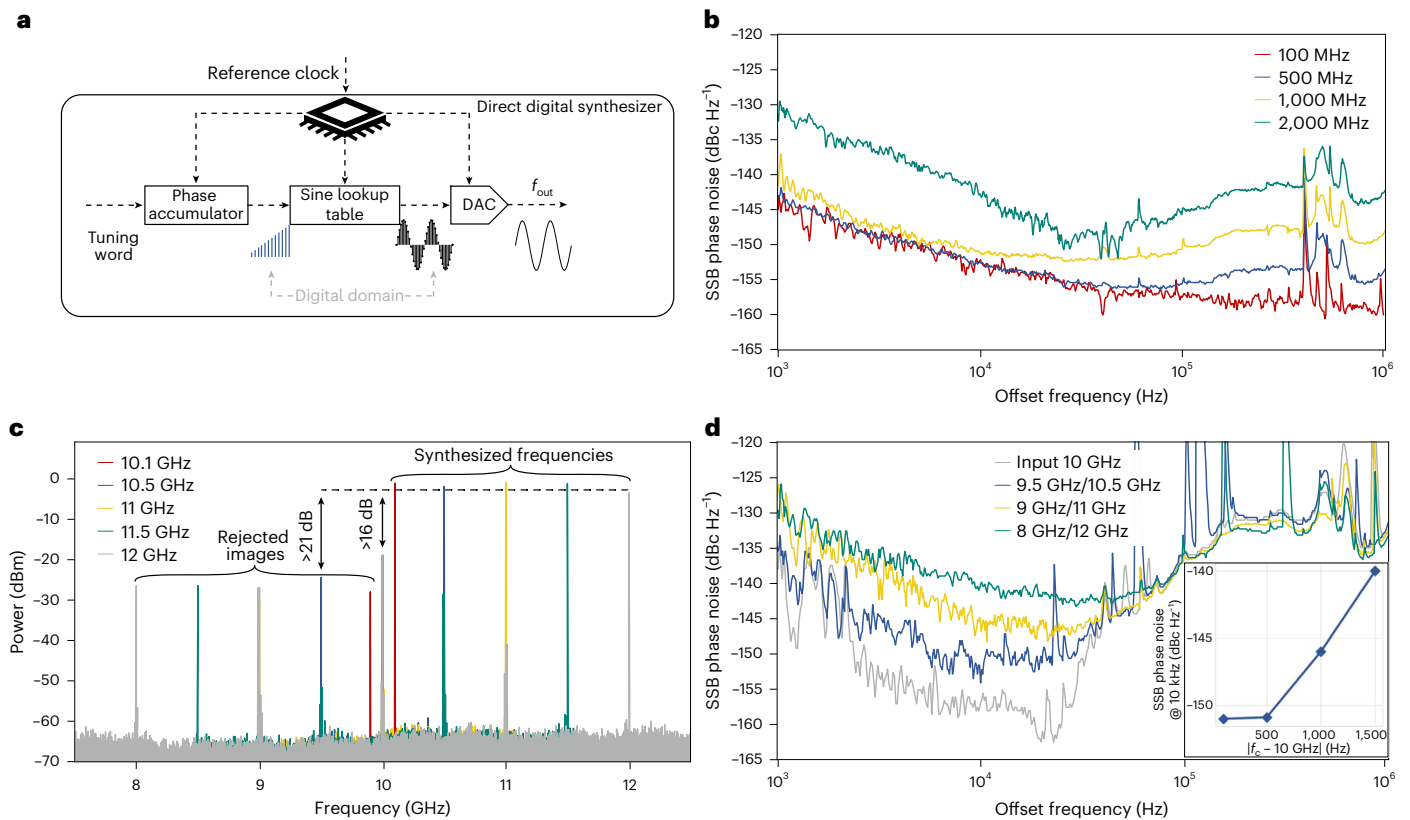


Fig. 3 | Synthesizer performance. **a**, DDS architecture. **b**, SSB phase noise of DDS output in the range from 100 MHz to 2 GHz, when the stabilized 10 GHz serves as an external clock. **c**, RF spectra of the synthesized frequencies. The spectrum

with the lower synthesized frequencies is exactly symmetric to the presented one. **d**, SSB phase noise of the synthesized frequencies from 8 to 12 GHz. Inset, phase noise at 10 kHz offset against the synthesized frequency.

to provide a 90° phase shift between the I and Q ports of the mixer. The phase shift of 90° is necessary to achieve single-sideband (SSB) operation with high image rejection. Output in the range 8–10 GHz or 10–12 GHz is determined by the relative sign of the phase shift between the I and Q ports.

Power spectra of synthesized frequencies in the 10–12 GHz band are shown in Fig. 3c. The rejection of the synthesized frequencies relative to the original 10 GHz carrier is more than 16 dB across all tuning frequencies. This rejection can be increased by using a higher power to drive the I and Q inputs of the mixer. Image rejection exceeded 21 dB across all generated frequencies. This rejection can be improved with more precise amplitude balance and phase control between the I and Q ports. Alternatively, one could use two DDSs, clocked by the same microwave input, with precise digital tuning of the amplitude and respective phases adjusted to 90° .

Figure 3d shows our measurements of the phase noise of the synthesized frequencies at discrete values across the entire X-band. At offsets above 80 kHz, the phase noise is limited by the noise of the 10 GHz signal itself, whereas at lower offset frequencies, the noise from the DDS dominates, which correlates well with the phase-noise measurements of the DDS. The noise on the synthesized frequencies in the range 9.5 to 10.5 GHz falls below -150 dBc Hz $^{-1}$ at 10 kHz offset, whereas the phase noise increases to near -140 dBc Hz $^{-1}$ at 8 and 12 GHz. Note, that the downscaled clock noise does not affect the synthesizer output noise, as the noise of the original 10 GHz is higher than its downscaled replica. However, the flicker noise in the analogue circuitry, along with quantization noise and DAC nonlinearity of the DDS, limit the reduction of clock noise.

This increase versus carrier frequency (f_c) is summarized in the inset in Fig. 3d. The phase-noise contribution of the DDS to the entire synthesizer can be categorized into two regions. In the range 9.5 to 10.5 GHz,

the phase noise does not depend on the carrier frequency. However, at carrier frequencies offset by more than 500 MHz from 10 GHz, the phase noise increases approximately as $20 \log(N)$, where N is the frequency multiplication factor. Considering the noise sources described earlier, we assume that the dominant noise source at carrier frequencies closer to 10 GHz is quantization noise in the digital-to-analogue conversion. This noise results from the quantized number of DAC bits and the symbol rate of the DAC, which exhibits white noise power spectral density independent of the generated output frequency. Meanwhile, the noise originating within the final output stage of the DAC is likely the limitation at higher synthesized frequencies. This noise arises from both the DAC switching mechanism and the flicker noise of the output stages. The flicker noise from the analogue output stages exhibits a $1/f$ characteristic and scales with the generated output frequency. The switching noise occurs when the digital circuitry within the DAC changes state, leading to additional noise and spurs, particularly at high clock and output frequencies. Note that, as the noise is primarily limited by the DDS, there is no need for a reference microwave source with noise lower than the internal noise of the DDS, making 2P-OFD an ideal technique for such a synthesis approach.

An advantage of our approach is its versatility, which allows it to overcome the limited tunability of photonic-based microwave generators. We expect that similar phase-noise performance can be readily achieved in other microwave bands. For example, by using the 20 GHz harmonic from the photodetected EO comb, it is possible to partially cover the K-band while maintaining low noise, like what is depicted in Fig. 3d. The tuning resolution of the DDS is in the microhertz range, and it can be controlled at speeds of tens of nanoseconds²⁰. Compared to previous works on tunable microwave generation with a frequency comb^{19,20}, we demonstrate a fourfold improvement in the tunability with up to 10 dB improvement in phase noise. Moreover, by using

a bipolar complementary metal-oxide-semiconductor (Bi-CMOS) process that combines low-noise heterojunction bipolar transistors and high-speed CMOS transistors for digital operations, a fully on-chip optically driven electronic synthesizer is feasible. This method should achieve phase-noise performance comparable to the current design, while substantially reducing both the physical size and power consumption.

Conclusions

We have described a tunable low-noise microwave synthesizer using 2P-OFD in combination with DDS. Using 2P-OFD, we generate 10 GHz microwave signals with low noise on short or long timescales with a frequency instability of 1×10^{-13} at 0.1 s and phase noise of -156 dBc Hz $^{-1}$ at 10 kHz offset. With recent progress in hybrid and heterogeneous chip-scale integration of the photonic components, including the lasers^{26,27}, comb generators^{28–30}, miniature reference cavities³¹ and photodetectors³², it is now possible to achieve 2P-OFD using only components amenable to on-chip integration and, thus, to realize a complete microwave synthesizer on a chip^{17,18,21–23,25}. We show that 2P-OFD can be used to generate signals with broad frequency tunability while maintaining low phase noise. This is achieved by using the stabilized 10 GHz signal as the clock of a DDS. For synthesized frequencies in the range 8 to 12 GHz, the system exhibits phase noise of -140 dBc Hz $^{-1}$ at 10 kHz offset, whereas in the range 9.5–10.5 GHz, the phase noise is below -150 dBc Hz $^{-1}$. Although other systems have demonstrated lower phase noise^{13,15}, they are not frequency tunable and require hardware that cannot be integrated on chip. When compared to existing 2P-OFD (at a fixed 10 GHz frequency), we achieved phase noise on par with the best discrete-component systems²⁴, but also achieve full 8–12 GHz tunability and low oscillator instability. The performance of our synthesizer could be further improved by optimizing the system with a lower-noise DDS and lasers, larger OFD factors, and improved servo systems. Additionally, by using lower-noise RF amplifiers, it is possible to access low-noise microwaves with power above +30 dBm (Methods). These insights provide a route for low size, weight and power photonic microwave generation with low-noise and broad tunability, as will be important for multiple applications in navigation, communications and sensing.

Methods

High-power output

To access the high-power 10 GHz, we used one of the termination ports of the EO modulators, as shown in Extended Data Fig. 1. Each termination port provided a 10 GHz signal with power of more than 1 W. The phase noise of the high-power 10 GHz is shown in Extended Data Fig. 2. The phase noise reached -149 dBc Hz $^{-1}$ at 10 kHz offset, limited by the noise from other amplifiers, as discussed in the main text. Thus, by using a lower-noise RF amplifier, it would be possible to generate low-noise 10 GHz with power above 1 W and performance matching that presented in the main text.

Measurement of the relative stability of the reference lasers

Extended Data Fig. 3 illustrates the experimental set-up used to measure the relative stability of the reference lasers. The approach is like 2P-OFD, where the reference lasers beat with a frequency comb to generate f_{IF} . However, to measure the relative phase noise of the lasers, an independent fully stabilized frequency comb was used as a reference. First, the two reference lasers were optically combined using a 2×2 optical coupler. The coupler outputs were then separately combined with two different fully stabilized reference optical frequency combs. By using two reference frequency combs, we were able to cross-correlate the phase noise, thus eliminating the noise of the frequency combs and photodetector noise. Both combs and the lasers were spectrally divided in wavelength-division multiplexers and photodetected to provide two beat notes for each comb. These beat

notes were filtered, amplified and mixed to provide two f_{IF} values for each comb. Both f_{IF} values were mixed down to the same frequency to perform the cross-correlation with a commercial phase noise analyser.

Data availability

All data for the figures in this manuscript are available via Figshare at <https://doi.org/10.6084/m9.figshare.27000427.v1> (ref. 48).

References

1. Townes, C. H. & Schawlow, A. L. *Microwave Spectroscopy* (Courier Corporation, 2013).
2. Sullivan, W. T. *Classics in Radio Astronomy*, Vol. 10 (Springer Science & Business Media, 2012).
3. Khanzadi, M. R. *Phase Noise in Communication Systems—Modeling, Compensation, and Performance Analysis* (Chalmers Univ. of Technology, 2015).
4. Razavi, B. & Behzad, R. *RF Microelectronics*, Vol. 2 (Prentice Hall, 2012).
5. Armada, A. G. Understanding the effects of phase noise in orthogonal frequency division multiplexing (OFDM). *IEEE Trans. Broadcast.* **47**, 153–159 (2001).
6. Serafino, G. et al. Toward a new generation of radar systems based on microwave photonic technologies. *J. Lightwave Technol.* **37**, 643–650 (2019).
7. Ghelfi, P. et al. A fully photonics-based coherent radar system. *Nature* **507**, 341–345 (2014).
8. McKinney, J. D. Photonics illuminates the future of radar. *Nature* **507**, 310–312 (2014).
9. Skolnik, M. I. et al. *Introduction to Radar Systems*, Vol. 19621 (McGraw-Hill, 2001).
10. Krieger, G. & Younis, M. Impact of oscillator noise in bistatic and multistatic SAR. *IEEE Geosci. Remote Sens. Lett.* **3**, 424–428 (2006).
11. Diddams, S. et al. Design and control of femtosecond lasers for optical clocks and the synthesis of low-noise optical and microwave signals. *IEEE J. Sel. Top. Quantum Electron.* **9**, 1072–1080 (2003).
12. Fortier, T. M. et al. Generation of ultrastable microwaves via optical frequency division. *Nat. Photonics* **5**, 425–429 (2011).
13. Xie, X. et al. Photonic microwave signals with zeptosecond-level absolute timing noise. *Nat. Photonics* **11**, 44–47 (2017).
14. Nakamura, T. et al. Coherent optical clock down-conversion for microwave frequencies with 10^{-18} instability. *Science* **368**, 889–892 (2020).
15. Elyahu, D., Seidel, D. & Maleki, L. Phase noise of a high performance OEO and an ultra low noise floor cross-correlation microwave photonic homodyne system. In *Proc. 2008 IEEE International Frequency Control Symposium* 811–814 (IEEE, 2008).
16. Swann, W. C., Baumann, E., Giorgetta, F. R. & Newbury, N. R. Microwave generation with low residual phase noise from a femtosecond fiber laser with an intracavity electro-optic modulator. *Opt. Express* **19**, 24387–24395 (2011).
17. Li, J., Yi, X., Lee, H., Diddams, S. A. & Vahala, K. J. Electro-optical frequency division and stable microwave synthesis. *Science* **345**, 309–313 (2014).
18. Kudelin, I. et al. Photonic chip-based low-noise microwave oscillator. *Nature* **627**, 534–539 (2024).
19. Fortier, T. et al. Optically referenced broadband electronic synthesizer with 15 digits of resolution. *Laser Photonics Rev.* **10**, 780–790 (2016).
20. Wei, J., Kwon, D., Zhang, S., Pan, S. & Kim, J. All-fiber-photonics-based ultralow-noise agile frequency synthesizer for X-band radars. *Photonics Res.* **6**, 12–17 (2018).
21. Sun, S. et al. Integrated optical frequency division for microwave and mmWave generation. *Nature* **627**, 540–545 (2024).

22. Zhao, Y. et al. All-optical frequency division on-chip using a single laser. *Nature* **627**, 546–552 (2024).
23. Jin, X. et al. Microresonator-referenced soliton microcombs with zeptosecond-level timing noise. Preprint at arxiv.org/abs/2401.12760 (2024).
24. Li, J. & Vahala, K. Small-sized, ultra-low phase noise photonic microwave oscillators at X-Ka bands. *Optica* **10**, 33–34 (2023).
25. He, Y. et al. Chip-scale high-performance photonic microwave oscillator. *Sci. Adv.* [10.1126/sciadv.ado9570](https://doi.org/10.1126/sciadv.ado9570) (2024).
26. Jin, W. et al. Hertz-linewidth semiconductor lasers using CMOS-ready ultra-high-Q microresonators. *Nat. Photonics* **15**, 346–353 (2021).
27. Xiang, C. et al. 3D integration enables ultralow-noise isolator-free lasers in silicon photonics. *Nature* **620**, 78–85 (2023).
28. Shen, B. et al. Integrated turnkey soliton microcombs. *Nature* **582**, 365–369 (2020).
29. Zhang, M. et al. Broadband electro-optic frequency comb generation in a lithium niobate microring resonator. *Nature* **568**, 373–377 (2019).
30. Xiang, C. et al. Laser soliton microcombs heterogeneously integrated on silicon. *Science* **373**, 99–103 (2021).
31. Cheng, H. et al. A novel approach to interface high-Q Fabry–Pérot resonators with photonic circuits. *APL Photonics* **8**, 116105 (2023).
32. Zhang, J. et al. Reduction of amplitude-to-phase conversion in charge-compensated modified unitraveling carrier photodiodes. *J. Lightwave Technol.* **36**, 5218–5223 (2018).
33. Drever, R. W. et al. Laser phase and frequency stabilization using an optical resonator. *Appl. Phys. B* **31**, 97–105 (1983).
34. Häfner, S. et al. 8×10^{-17} fractional laser frequency instability with a long room-temperature cavity. *Opt. Lett.* **40**, 2112–2115 (2015).
35. Álvarez, M. D. *Optical Cavities for Optical Atomic Clocks, Atom Interferometry and Gravitational-wave Detection* (Springer, 2019).
36. Matei, D. et al. 1.5 μm lasers with sub-10MHz linewidth. *Phys. Rev. Lett.* **118**, 263202 (2017).
37. McLemore, C. A. et al. Miniaturizing ultrastable electromagnetic oscillators: sub- 10^{-14} frequency instability from a centimeter-scale Fabry–Perot cavity. *Phys. Rev. Appl.* **18**, 054054 (2022).
38. Kelleher, M. L. et al. Compact, portable, thermal-noise-limited optical cavity with low acceleration sensitivity. *Opt. Express* **31**, 11954–11965 (2023).
39. Parriaux, A., Hammani, K. & Millot, G. Electro-optic frequency combs. *Adv. Opt. Photonics* **12**, 223–287 (2020).
40. Liu, Y. et al. Low-noise microwave generation with an air-gap optical reference cavity. *APL Photonics* **9**, 010806 (2024).
41. Groman, W. et al. Photonic millimeter-wave generation beyond the cavity thermal limit. *Optica* **11**, 1583–1587 (2024).
42. Loh, W. et al. Ultralow noise microwave synthesis via difference frequency division of a Brillouin resonator. *Optica* **11**, 492–497 (2024).
43. Chen, L. et al. Vibration-induced elastic deformation of Fabry–Perot cavities. *Phys. Rev. A* **74**, 053801 (2006).
44. Nazarova, T., Riehle, F. & Sterr, U. Vibration-insensitive reference cavity for an ultra-narrow-linewidth laser. *Appl. Phys. B* **83**, 531–536 (2006).
45. Fortier, T. M. et al. Photonic microwave generation with high-power photodiodes. *Opt. Lett.* **38**, 1712–1714 (2013).
46. Murphy, E. & Slattery, C. Ask the application engineer—33 all about direct digital synthesis. *Analog Dialogue* **38**, 8–12 (2004).
47. Calosso, C. E., Gruson, Y. & Rubiola, E. Phase noise and amplitude noise in DDS. In *Proc. 2012 IEEE International Frequency Control Symposium 1–6* (IEEE, 2012).
48. Kudelin, I. et al. Data for manuscript entitled ‘An optoelectronic microwave synthesizer with frequency tunability and low phase noise’. *Figshare* <https://doi.org/10.6084/m9.figshare.27000427.v1> (2024).

Acknowledgements

We thank K. Chang and N. Hoghooghi for their comments on the manuscript. Commercial equipment and trade names are identified for scientific clarity only, and doing so does not represent an endorsement by NIST. This research was supported by the DARPA GRYPHON programme (Grant No. HR0011-22-2-0009 to J.C.C., S.M.B., F.Q. and S.A.D.), NIST (F.Q.) and the University of Colorado Boulder (S.A.D.).

Author contributions

S.M.B, F.Q. and S.A.D. conceived the experiment and supervised the project. I.K. and S.A.D. wrote the paper with input from all authors. I.K., A.L. and W.G. built the experimental set-up. I.K. and D.M. performed the experiments. M.L.K. and F.Q. built the FP cavity. P.S., S.H., I.K. and S.M.B. built the RF synthesizer. D.L., T.N., C.A.M. and F.Q. provided the optically derived microwave reference and aided with the microwave phase-noise measurement system. J.B. and J.C.C. provided the modified uni-travelling carrier detectors. All authors contributed to the system design and discussion of the results.

Competing interests

The authors declare no competing interests.

Additional information

Extended data is available for this paper at <https://doi.org/10.1038/s41928-024-01294-x>.

Correspondence and requests for materials should be addressed to Igor Kudelin or Scott A. Diddams.

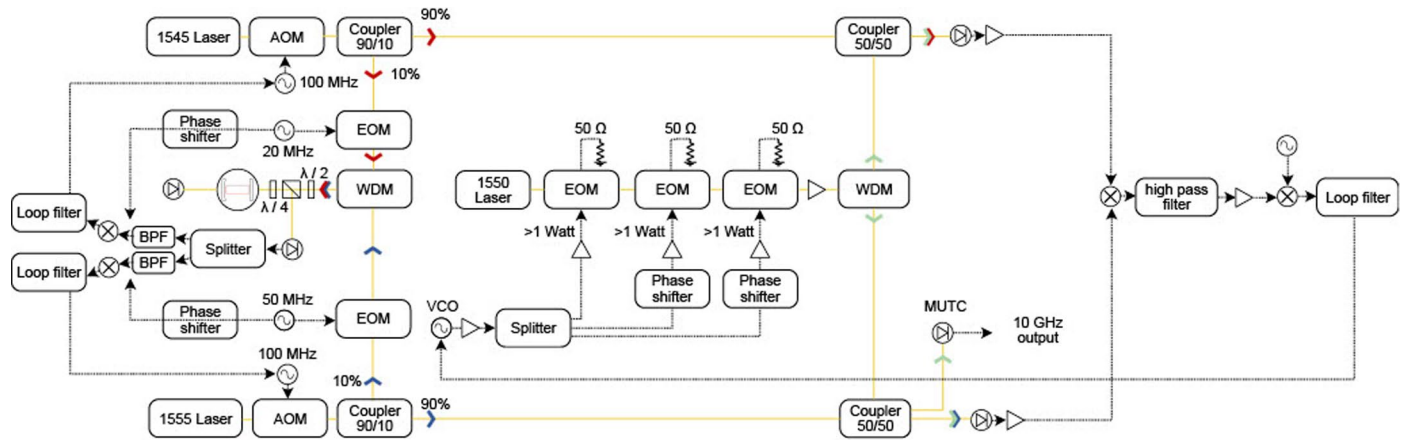
Peer review information *Nature Electronics* thanks Seung-Woo Kim and the other, anonymous, reviewer(s) for their contribution to the peer review of this work.

Reprints and permissions information is available at www.nature.com/reprints.

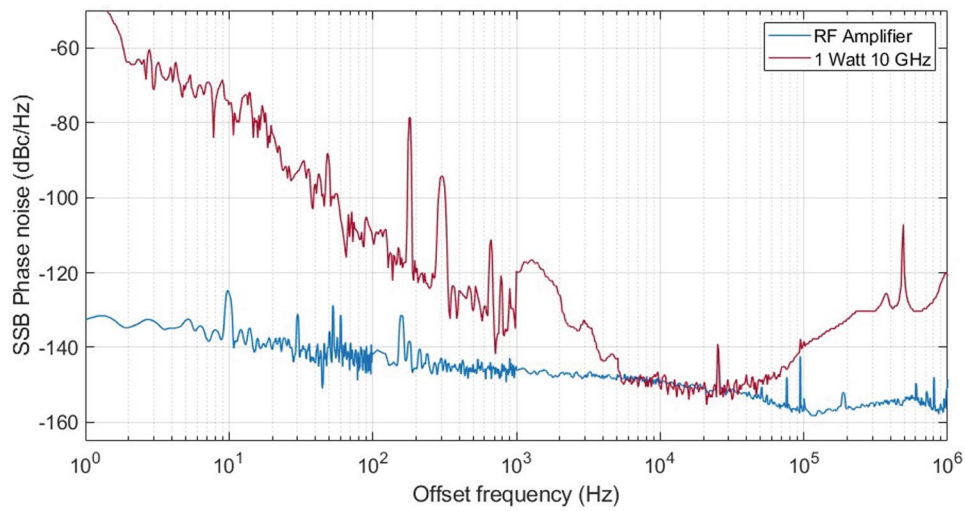
Publisher’s note Springer Nature remains neutral with regard to jurisdictional claims in published maps and institutional affiliations.

Springer Nature or its licensor (e.g. a society or other partner) holds exclusive rights to this article under a publishing agreement with the author(s) or other rightsholder(s); author self-archiving of the accepted manuscript version of this article is solely governed by the terms of such publishing agreement and applicable law.

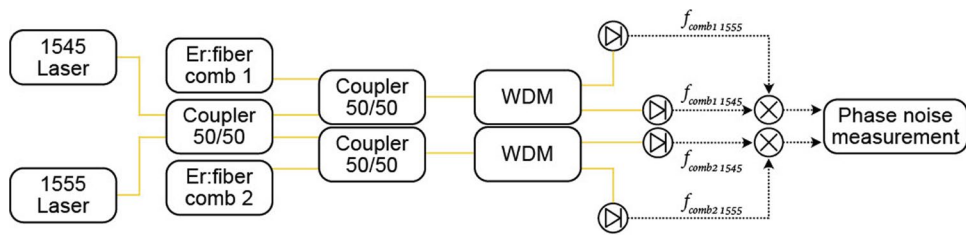
© The Author(s), under exclusive licence to Springer Nature Limited 2024



Extended Data Fig. 1 | A detailed schematic of the experimental setup. Instead of external 50 Ohm terminators, the RF signal at the EOM output can be used as a high-power output.



Extended Data Fig. 2 | High power output. Phase noise of the used RF amplifiers (blue) and high power 10 GHz signal from the EOM output (red). The peaks around 1–5 kHz due to unresolved harmonics of 60 Hz.



Extended Data Fig. 3 | Experimental setup to measure the relative phase noise of reference lasers by using two stabilized frequency combs. Both reference Er: fiber combs are fully stabilized.